analytica

MDPI

Article

Facile Synthesis of Elongated Cone-Shaped ZnO Nanostructure for Sensitive Cholesterol Biosensor Fabrication

Khansa Haneef [1], Rafiq Ahmad [2,*], Vandana Nagal [3], Abdullah [4], Kiesar Sideeq Bhat [5], Akil Ahmad [6], Mohammed B. Alshammari [6] and Byeong-Il Lee [1,7,8,*]

1 Industry 4.0 Convergence Bionics Engineering, Pukyong National University, Busan 48513, Republic of Korea; khansah@pukyong.ac.kr
2 'New-senior' Oriented Smart Health Care Education Center, Pukyong National University, Busan 48513, Republic of Korea
3 Department of Physics, Guru Jambheshwar University of Science & Technology, Hisar 125001, Haryana, India; vandananagal@gjust.org
4 Future Energy Convergence Core Center, Jeonbuk National University, Jeonju 54896, Republic of Korea; abdullahazmi@jbnu.ac.kr
5 Department of Applied Sciences (Chemistry), Institute of Technology, Zakura Campus, University of Kashmir, Hazratbal, Srinagar 190006, India; mayorkaiser89@gmail.com
6 Department of Chemistry, College of Science and Humanities in Al-Kharj, Prince Sattam Bin Abdulaziz University, Al-Kharj 11942, Saudi Arabia; aj.ahmad@psau.edu.sa (A.A.); m.alshammari@psau.edu.sa (M.B.A.)
7 Digital Healthcare Research Center, Institute of Information Technology and Convergence, Pukyong National University, Busan 48513, Republic of Korea
8 Division of Smart Healthcare, College of Information Technology and Convergence, Pukyong National University, Busan 48513, Republic of Korea
* Correspondence: rahmad5@pknu.ac.kr (R.A.); bilee@pknu.ac.kr (B.-I.L.)

Abstract

Elevated cholesterol levels are closely associated with cardiovascular disease. Therefore, rapid and accurate detection is essential for early diagnosis, effective disease management, and improved clinical outcomes. In this work, we synthesised elongated cone-shaped zinc oxide nanostructures (ZnO NSs) on the working electrode via a facile hydrothermal route and characterized. The synthesized elongated cone-shaped ZnO NSs were used to fabricate a cholesterol biosensor. This work describes the fabrication process and analytical performance characteristics of the cholesterol biosensor in detail. The biosensing performance was electrochemically analysed using cholesterol solutions prepared in a buffer medium. The biosensor sensitivity, linear range, and limit-of-detection were 0.398 μA μM^{-1} cm^{-2}, 5–600 μM, and 0.12 μM, respectively. The biosensor was insensitive to possible interfering analytes, reflecting its selectivity. Additionally, the biosensor showed good stability, reproducibility, and practical applicability. This work demonstrates a simple route to fabricate a sensitive cholesterol biosensor, with the potential to further improve biosensing performance by modifying the surface of the cone-shaped ZnO NSs with highly electroactive nanomaterials.

Keywords: facile synthesis; cone-shaped ZnO; hydrothermal route; biosensor; cholesterol detection

Check for updates

Academic Editors: Stella Girousi, Rigini M. Papi and Pavlos Tziourrou

Received: 21 October 2026
Revised: 17 November 2026
Accepted: 19 November 2026
Published: 26 November 2026

Copyright: © 2026 by the authors. Licensee MDPI, Basel, Switzerland. This article is an open access article distributed under the terms and conditions of the Creative Commons Attribution (CC BY) license.

1. Introduction

Cholesterol ($C_{27}H_{48}O_2$) is an essential lipid biomolecule produced in the liver and plays a fundamental role in various bodily activities, including membrane fluidity, integrity, and permeability [1]. It is also a key precursor in cholesterol metabolism, making cholesterol indispensable for normal physiological functions [2,3]. Blood cholesterol concentration below

200 mg dL^{-1} (<5.2 mM) is generally considered desirable for healthy individuals [4]. However, elevated cholesterol levels (more than 240 mg dL^{-1} (>6.2 mM); hypercholesterolemia) are associated with an increased risk of hypertension and cardiovascular diseases [5,6]. Also, abnormally low cholesterol levels (hypocholesterolemia) are linked to various health conditions, including malabsorption syndromes, anemia, hyperthyroidism, and other physiological abnormalities [4,7,8]. Cholesterol comes from both dietary intake and endogenous synthesis in the liver. Therefore, accurate monitoring of its concentration in biological fluids and food products is crucial for early disease diagnosis, effective clinical management, and preventive healthcare.

Researchers use different analytical techniques to determine cholesterol concentration in biological and food samples. For example, colorimetry, spectrophotometry, liquid chromatography, immunosorbent assays, fluorescent, and electrogenerated chemiluminescence [9–13]. These methods provide reliable analytical performance but have several drawbacks, including complex sample preparation, the need for skilled personnel and expensive instrumentation, and long analysis times, which limit their applicability for rapid and point-of-care testing [14]. However, electrochemical biosensors overcome these limitations and have emerged as an attractive alternative, offering rapid response, high sensitivity and selectivity, cost-effectiveness, and ease of use [15–17]. Developing highly sensitive, selective, and cost-effective electrochemical cholesterol biosensors is important for clinical diagnostics and real-time health monitoring.

To improve the analytical performance of electrochemical biosensors, researchers have focused on developing nanostructured materials through advances in nanotechnology and nanoengineering [18–22]. The nanomaterials with tunable physicochemical properties have been synthesised and used in biosensor fabrication, exhibiting a high surface-to-volume ratio, superior electrical conductivity, and enhanced catalytic activity, facilitating efficient electron transfer and biomolecule immobilization [22]. Thereby, the utilization of nanomaterials improves the sensitivity, selectivity, and overall analytical performance of electrochemical biosensors. To date, various nanomaterials, including carbon-based, organic, inorganic, and composite materials, have been widely incorporated to optimize performance of electrochemical sensors [23–25]. Among them, metal oxide nanostructures have attracted significant attention for developing next-generation cholesterol biosensors for biomedical applications, particularly cholesterol monitoring, owing to their excellent electrical, catalytic, and structural properties [25,26].

Among metal oxides, ZnO has emerged as a promising material for electrochemical sensors because of its excellent biocompatibility, high isoelectric point, large surface area, and superior electron-transport properties [27]. ZnO has been synthesized in diverse nanostructured forms, including nanoparticles, nanorods, nanowires, nanosheets, and nanospheres, to enhance sensor performance [28]. While ZnO has been employed in both enzymatic and non-enzymatic cholesterol sensors, its high enzyme immobilization capability makes it particularly attractive for enzymatic biosensors, which offer superior sensitivity, selectivity, and analytical performance in complex biological samples [29]. To further improve biosensor performance, composites, hierarchical nanostructures, and multi-enzyme cascade reactions have attracted attention because of their high specific surface area, interconnected architecture, enhanced physicochemical properties, and enzyme catalysis supported by functional materials [19,30–34]. These features facilitate efficient electron transfer and increased biomolecule loading, resulting in superior sensing performance compared with conventional nanostructures.

Recent advances in nanotechnology, materials science, and enzyme engineering have significantly improved the analytical performance of electrochemical-based cholesterol biosensors by enhancing sensitivity, selectivity, and operational stability [35]. Nevertheless,

long-term stability and reproducibility remain major challenges. To address these issues, researchers have focused on directly growing nanostructures on electrode surfaces, particularly via low-temperature hydrothermal methods, which offer a simple, cost-effective, and scalable fabrication approach [36–38]. Among other nanomaterials, ZnO is especially attractive due to its excellent biocompatibility and ability to form well-aligned, vertically oriented nanostructures that facilitate efficient electron transfer, robust enzyme immobilization, and improved sensing performance [36–39]. Therefore, rationally designing novel ZnO architectures is essential for developing high-performance biosensors.

Herein, we report the facile hydrothermal synthesis of elongated cone-shaped zinc oxide (ZnO) nanostructures on the working electrode to fabricate an electrochemical cholesterol biosensor. The electrochemical sensing performance of the Nf/ChOx/ZnO NSs/Ag/Si biosensor was evaluated for cholesterol detection. The biosensor's selectivity, storage stability, fabrication reproducibility, and practical applicability were assessed. The findings show that elongated cone-shaped ZnO NSs provide an effective platform for cholesterol biosensor fabrication and have further potential for use in other biosensor fabrication, either by modifying their surface with analyte-specific enzymes or with electroactive nanomaterials.

2. Materials and Methods

2.1. Reagents

Hexamethylenetetramine (HMTA, ≥99%), Nafion (Nf, 5 wt%), cholesterol oxidase (ChOx) from microorganisms (lyophilized powder, ≥50 units/mg protein), zinc nitrate hexahydrate ($Zn(NO_3)_2{\cdot}6H_2O$, 98%), cholesterol-water soluble (powder, BioReagent), dopamine (DA, ≥98%), D-(+)-glucose (≥99.5%), uric acid (UA, ≥99%), human serum (H4522), ascorbic acid (AA, 99%), fructose (≥99%), L-cysteine (L-Cyst, ≥98%), sucrose (≥99.5%), and phosphate buffered saline (PBS, liquid, pH = 7.4) were purchased from Sigma-Aldrich (Burlington, MA, USA). Solutions were prepared using ultrapure water (18.2 MΩ·cm) obtained from a Milli-Q water purification system.

2.2. Elongated Cone-Shaped ZnO NSs-Based Cholesterol Biosensor Fabrication

Figure 1 illustrates the fabrication steps for the elongated cone-shaped ZnO NSs-based cholesterol biosensor. Silicon (Si) substrates (5 × 0.4 cm) were cut using a diamond cutter. The substrates were sequentially ultrasonicated in acetone, isopropanol, and deionized water to remove surface contaminants, followed by drying under a nitrogen stream (i). The cleaned substrates were then heated at 120 °C for 10 min to remove residual moisture before depositing the silver (Ag) electrode. The Ag film (~150 nm) was then deposited onto the cleaned Si substrate in a nitrogen atmosphere using RF magnetron sputtering (Ag target purity, 99.99%; RF power, 60 W) (ii). Next, a ZnO seed (~60 nm) layer was sputtered on the selected area (0.4 × 0.4 cm) using a 99.99% pure ZnO target and 60 W RF power in an argon atmosphere, while the remaining substrate surface was masked with tape (iii). The sputtering chamber pressure was maintained at 2.6×10^{-3} Torr for Ag and 6.5×10^{-3} Torr for ZnO seed deposition.

A facile low-temperature hydrothermal route was used to synthesize the elongated cone-shaped ZnO NSs on a ZnO-seed/Ag/Si electrode (iv). Briefly, the seeded substrate was positioned inverted, with the active surface facing downward and tilted (~45°), in a Pyrex reaction vessel containing an aqueous precursor solution of 0.2 M $Zn(NO_3)_2{\cdot}6H_2O$ and 0.2 M HMTA. Hydrothermal growth was allowed to proceed at 95 °C for 10 h, following which the electrode (elongated cone-shaped ZnO NSs/Ag/Si) was repeatedly rinsed with deionized water to remove residual reactants and dried.

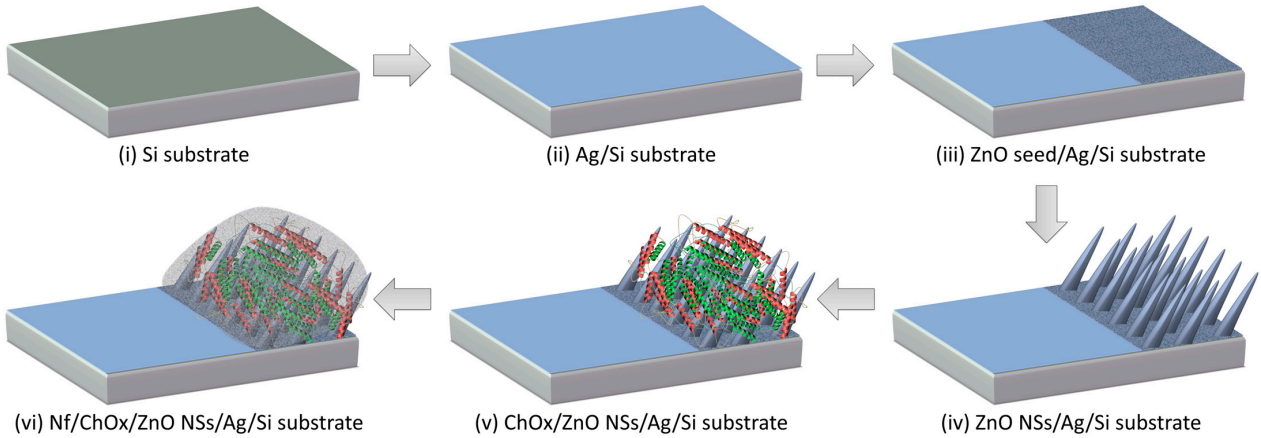

Figure 1. Cholesterol biosensor fabrication steps: (**i**) Si substrate cleaning, (**ii**) deposition of Ag on the Si substrate, (**iii**) deposition of ZnO seed layer in selected area, (**iv**) hydrothermal growth of cone-shaped ZnO NSs, (**v**) ChOx immobilization, and (**vi**) Nf membrane covering.

Before ChOx enzyme immobilization, the elongated cone-shaped ZnO NSs/Ag/Si electrode was dipped into PBS buffer (pH = 7.4) for 5 min to increase surface hydroxylation and improve hydrophilicity, thereby facilitating enzyme attachment. The ChOx enzyme (5.0 mg/mL) was prepared in 0.1 M PBS buffer (pH = 7.4), and 10 µL of ChOx was dropped onto the elongated cone-shaped ZnO NSs/Ag/Si electrode surface, then incubated for 12 h at 4 °C (v). The enzyme-immobilized electrode (ChOx/ZnO NSs/Ag/Si) was gently rinsed with PBS buffer to remove excess unimmobilized ChOx. Finally, 2 µL of 0.5 wt% Nf was coated over the ChOx-immobilized electrode to improve enzyme retention, suppress interfering species, and enhance the biosensor's operational stability (vi).

2.3. Apparatus

The morphology and structural characteristics of the synthesized elongated cone-shaped ZnO NSs were investigated using FESEM (Hitachi S-4700, Tokyo, Japan) equipped with EDS and TEM/HRTEM (JEM-2010, JEOL Ltd., Tokyo, Japan). The crystal structure was examined by X-ray diffraction (XRD, Rigaku, The Woodlands, TX, USA) using Cu-Kα radiation (λ = 1.5418 Å) over a 2θ range of 30–50° at a scanning rate of 5° min^{-1}. The optical properties were characterized by Raman spectroscopy (JASCO NRS-5100, JASCO Co. Ltd., Tokyo, Japan; 532 nm Ar^{+} laser).

Electrochemical measurements were performed at room temperature using a PalmSens4 potentiostat (Houten, The Netherlands) in a conventional three-electrode configuration, with Nf/ChOx/ZnO NSs/Ag/Si (working), Ag/AgCl (reference), and a Pt wire (counter) electrode. CV and EIS measurements were carried out in an electrolyte containing 5 mM $K_3[Fe(CN)_6]/K_4[Fe(CN)_6]$ (1:1) and 0.1 M KCl in a potential range of −0.4–0.8 V and over a frequency range of 10^{-1}–10^{5} Hz (applied potential, 0.11 V), respectively. DPV was employed to evaluate the electrochemical response of the fabricated (Nf/ChOx/ZnO NSs/Ag/Si) biosensor to cholesterol. PBS (pH 7.4) was selected as the supporting electrolyte because the oxidation behavior of cholesterol is strongly influenced by the solution pH [40]. DPV measurements were performed over a potential window of +0.1–+0.7 V using the following optimized parameters: step potential of 0.005 V, pulse amplitude of 0.10 V, pulse width of 0.01s, and a scan rate of 50 mV/s.

3. Results

3.1. Characterization of Elongated Cone-Shaped ZnO NSs

The surface morphology of the synthesized elongated cone-shaped ZnO NSs was examined by FESEM. As shown in Figure 2a,b, the ZnO exhibited high-density growth and was uniformly distributed, with vertically aligned nanostructures. The cross-sectional FESEM image (Figure 2c) further confirmed vertical growth and an elongated, cone-shaped morphology, with lengths ranging from approximately 0.6 to 1.9 µm. In addition, the base of the ZnO NSs is thicker than the top, resulting in an elongated cone-shaped morphology with an increased active surface area. EDS was used to investigate the elemental composition of the elongated cone-shaped ZnO NSs. As shown in Figure 2d, the EDS spectrum confirms that zinc (Zn) and oxygen (O) are the major constituents of the ZnO NSs, while the Ag signal originates from the underlying electrode substrate. TEM analyses (Figure 3) further reveal the morphology and crystalline structure of the elongated, cone-shaped ZnO NSs. The TEM image (Figure 3a) confirms the formation of elongated cone-shaped ZnO NSs. The HRTEM image (Figure 3b) displays well-defined lattice fringes correspond to the (002) plane of hexagonal wurtzite ZnO (PCPDF #89-1397), confirming its crystalline nature [19]. Furthermore, the SAED pattern (inset; Figure 3a) shows distinct diffraction spots associated with the characteristic planes of wurtzite ZnO, further supporting its well-defined crystalline structure.

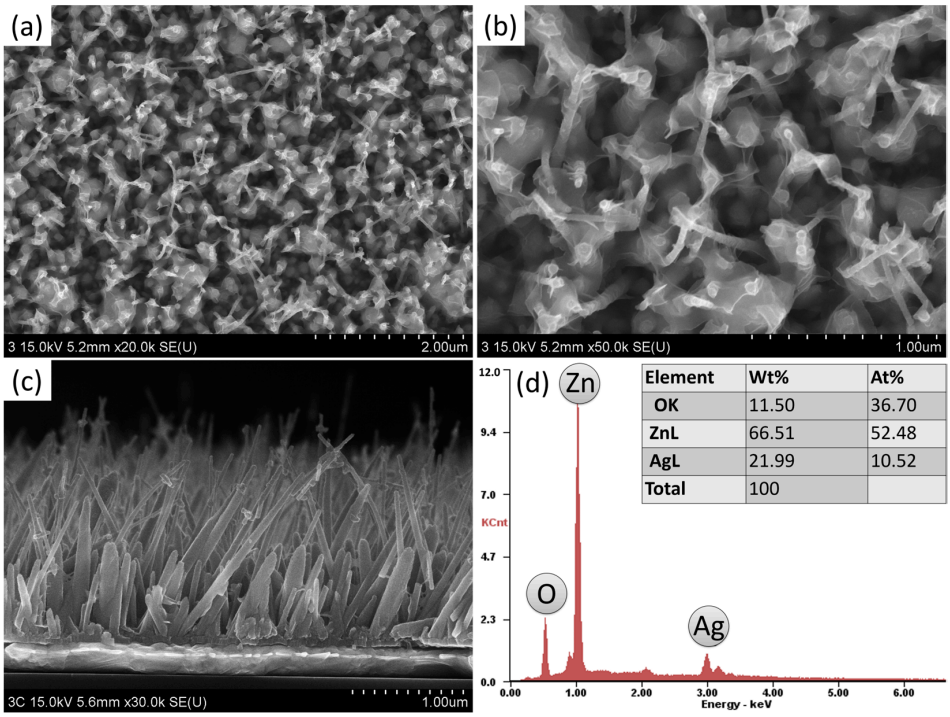

Figure 2. FESEM characterization of elongated cone-shaped ZnO NSs at low- (**a**) and high-magnification (**b**), along with cross-sectional FESEM image (**c**) and EDX analysis (**d**). Inset d shows the elemental composition table.

The structural characteristics and optical properties of the elongated cone-shaped ZnO NSs were systematically investigated using XRD and Raman spectroscopy (Figure 4). The XRD analysis showed diffraction peaks consistent with crystalline ZnO and matched JCPDS No. 35-1451, confirming phase-pure ZnO formation (Figure 4a). The intense (002) reflection indicates preferential growth along the c-axis, while the additional (111) and (200) reflections originate from the underlying sputtered Ag electrode (JCPDS No. 89-3722) [19]. The Raman spectrum showed a strong band at ~437 cm^{-1}, characteristic of the E_2 optical

phonon mode of wurtzite ZnO [41]. Weak bands at ~331 and 380 cm^{-1} were assigned to the E_{2H}-E_{2L} multiphonon process and A_1T mode, respectively, whereas the E_1L mode was barely detectable (Figure 4b). Overall, the XRD and Raman results confirm the formation of highly crystalline, phase-pure ZnO with a well-defined hexagonal wurtzite structure and preferential c-axis orientation.

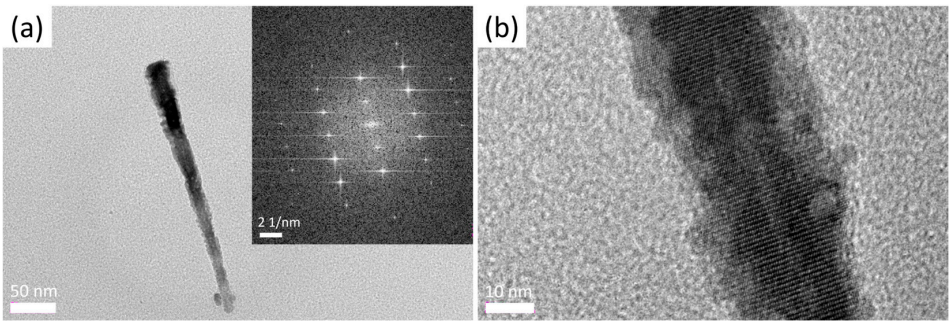

Figure 3. TEM (**a**) and HRTEM (**b**) images of the single elongated cone-shaped ZnO NS. Inset a shows the SAED pattern of the elongated cone-shaped ZnO NS.

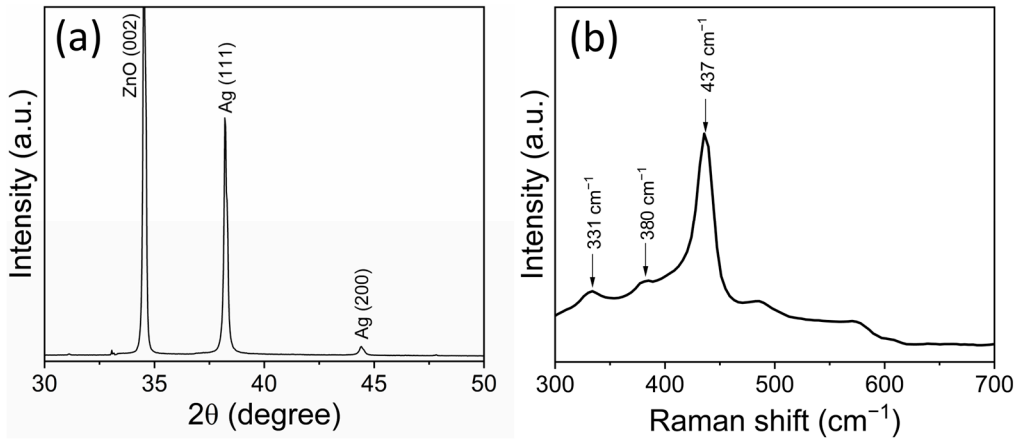

Figure 4. XRD (**a**) and Raman (**b**) spectra of elongated cone-shaped ZnO NSs.

3.2. Electrochemical Characterization of Fabricated Electrodes

The CV technique is a fundamental electrochemical technique used to investigate redox behavior, electron-transfer kinetics, and the electrochemical activity of electrode materials. Figure 5i shows the CV responses of the different electrode configurations (Ag/Si (a), ZnO seed/Ag/Si (b), ZnO NSs/ZnO seed/Ag/Si (c), and ChOx/ZnO NSs/ZnO seed/Ag/Si (d)) in a probe electrolyte. The bare Ag/Si electrode produced a higher redox current than the other electrodes (ZnO seed/Ag/Si (b), ZnO NSs/ZnO seed/Ag/Si (c), and ChOx/ZnO NSs/ZnO seed/Ag/Si (d). The histogram (Figure 5ii) shows a progressive decrease in current following ZnO seed deposition, ZnO NSs growth, and subsequent ChOx immobilisation. EIS further supported the CV findings by monitoring changes at the electrode–electrolyte interface during successive biosensor fabrication steps and assessing interfacial charge-transfer behaviour [42]. The EIS was measured to compare the electrochemical characteristics of the bare and modified electrodes and is presented in Figure 5iii. The Nyquist plots were fitted using a Randles equivalent circuit, and the corresponding charge-transfer resistance (Rct) was determined. The bare Ag/Si electrode exhibited a relatively low Rct of ~155 Ω, whereas deposition of the ZnO seed layer (~465 Ω), ZnO NSs growth (~1350 Ω), and subsequent ChOx immobilization (~2040 Ω) increased the Rct values (Figure 5iv). The increased Rct can be attributed to the relatively insulating ZnO

layer and the subsequent enzyme coating, which partially hinders direct electron transfer at the electrode–electrolyte interface. However, the ZnO nanostructures provide a high-surface-area platform for ChOx immobilization, enhance enzyme loading, and facilitate effective interaction with cholesterol molecules. Therefore, in the fabricated sensor, enzyme-mediated catalysis, rather than direct electron-transfer enhancement through the ZnO layer, primarily drives the sensing response. Overall, the increased resistance to electron transport at the modified interface agrees well with the observed current response in CV analysis.

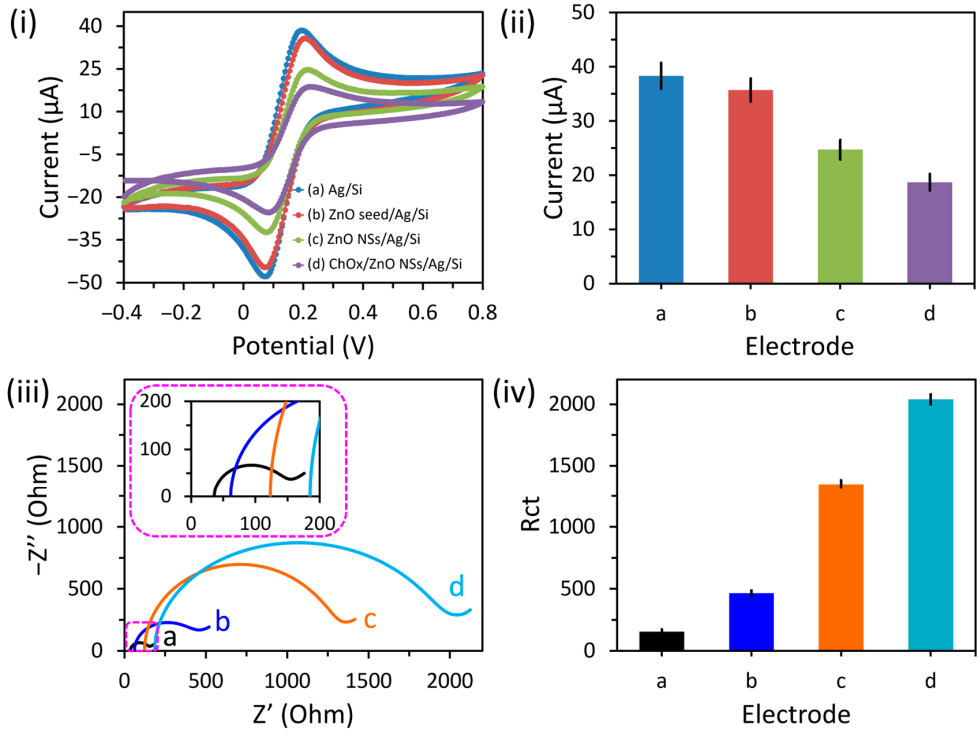

Figure 5. (**i**) CV responses and (**iii**) Nyquist plots obtained from EIS measurements of the different electrode configurations (a–d) in a probe electrolyte. (**ii**,**iv**) represent histograms of the CV peak current response and Rct value obtained during EIS measurements, respectively. The CV scan rate was set to 50 mV/s. EIS was performed in the 10^{-1}–10^{5} Hz frequency range with an applied potential of 0.11 V.

3.3. Analytical Testing of the Fabricated Biosensor in Cholesterol Detection

The fabricated Nf/ChOx/ZnO NSs/Ag/Si biosensor was used for cholesterol detection by DPV. Figure 6a shows DPV measurements in PBS buffer only, with no peak observed. Then, 50 µM cholesterol was added to the PBS buffer, and DPV analysis was performed. In the presence of cholesterol, the DPV response shows a well-defined oxidation peak at approximately +0.40 V versus Ag/AgCl. The cholesterol detection involves two sequential processes (Figure 6b). First, the ChOx catalyzes cholesterol oxidation in the presence of oxygen (O_2), generating cholest-4-en-3-one and hydrogen peroxide (H_2O_2) [43]. Then, the enzymatically generated H_2O_2 undergoes electrochemical oxidation at the electrode surface, producing the current response used to quantify cholesterol [44]. Thus, the measured electrochemical signal arises from oxidation of H_2O_2 generated during the enzymatic reaction rather than direct electrochemical oxidation of cholesterol.

The cholesterol biosensor (Nf/ChOx/ZnO NSs/Ag/Si) was evaluated at increasing cholesterol concentrations (5–700 µM). The DPV profiles showed an increase in oxidation peak current with increasing cholesterol concentration (Figure 6c). The peak current shows a concentration-dependent relationship with cholesterol concentration (inset; Figure 6d). A strong linear correlation coefficient (R^2) of 0.9961 was obtained between the DPV peak cur-

rent and cholesterol concentration over the 5–600 µM range (Figure 6d). The corresponding calibration curve was y = 0.0637x + 5.8455, where x is the cholesterol concentration (µM), and y is the measured current (µA). The biosensor showed a concentration-dependent increase in peak current and a linear range of 5 to 600 µM, demonstrating its effective quantitative response. The biosensor exhibited a sensitivity of 0.398 µA μM^{-1} cm^{-2}, calculated by dividing the calibration curve slope (0.0637 µA/µM) by the working electrode surface area (0.16 cm^2). The detection limit (DL) was estimated to be 0.12 µM at a signal-to-noise ratio of 3 (DL = 3σ/S; where σ and S represent the blank-signal standard deviation and calibration sensitivity, respectively) (right inset, Figure 6c). Table 1 summarizes the analytical performance of the proposed sensor alongside previously reported cholesterol biosensors. The present sensor exhibits a competitive sensitivity and detection range. The sensing performance of the sensor may be attributed to the elongated cone-shaped ZnO NSs that provide favorable surface characteristics for enzyme immobilization and electrochemical sensing. Their morphology may also improve enzyme accessibility and interactions between the sensing layer and the electrode. Consequently, the elongated cone-shaped ZnO NSs-based electrode exhibited enhanced sensitivity and improved detection capability, highlighting its potential for reliable cholesterol sensing at low analyte concentrations.

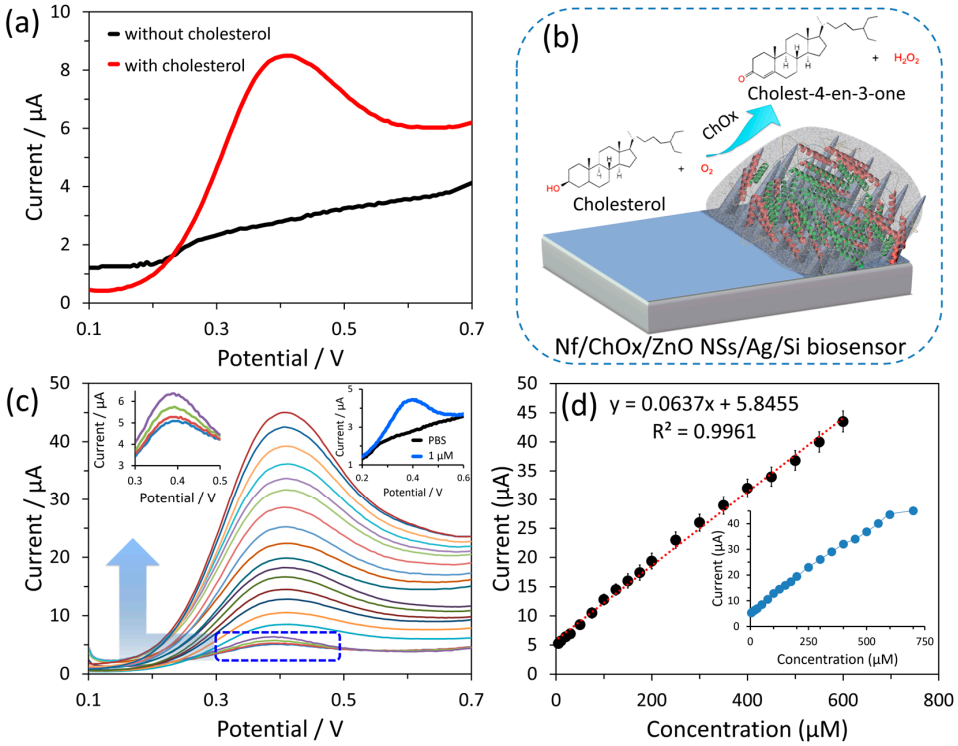

Figure 6. (**a**) DPV is used to analyse the oxidation current of cholesterol in the buffer without and with 50 µM cholesterol using the Nf/ChOx/ZnO NSs/Ag/Si biosensor; (**b**) oxidation mechanism showing electrochemical conversion of cholesterol in the presence of oxygen to cholest-4-en-3-one and H_2O_2; (**c**) DPV recorded in the presence of 5 to 700 µM cholesterol; (**d**) linear range calibration curve from 5 to 600 µM cholesterol concentrations (measurements were done in triplicate). Inset c (left) shows the recorded DPV response to 5, 10, 20, and 30 µM cholesterol concentrations. Inset c (right) shows the DPV curve in PBS without and with 1 µM cholesterol. Inset d shows the DPV response curves (linear and non-linear) as cholesterol concentration increases.

Table 1. Comparison of DPV-based electrochemical cholesterol biosensors.

Cholesterol Biosensor	Sensitivity ($\mu A \mu M^{-1} cm^{-2}$)	Detection Range (μM)	DL (μM)	Ref.
Chit/ChOx/Ti_3C_2Tx/GCE	0.13266	0.0003–0.0045	0.00011	[45]
HRP/ChOx/PTH/GCE	0.18	25–125	6.3	[46]
Nf/ChOx/GNPs-MWCNTs/GCE	-	10–5000	4.3	[47]
ChOx/PSS/PILs-GP/GCE	-	10.5–10400	3.5	[48]
ChOx/Au NPs/$CoFe_2O_4$@MoS_2/GCE	0.194	5–100	0.09	[49]
ChOx/Au/TiO_2/MWCNTs/FTO	50.066	0.05–80	0.0018	[50]
ChOx/Au/ZnO/MWC-NTs/FTO	25.89	0.1–100	0.1	[51]
Nf/ChOx/ZnO NSs/Ag/Si	0.398	5–600	0.12	This work

Abbreviations: Chit, chitosan; ChOx, cholesterol oxidase; GCE, glassy carbon electrode; PTH, poly(thionine); HRP, horseradish peroxidase; Nf, nafion; GNPs, gold nanoparticles; MWCNTs, multiwalled carbon nanotubes; PSS, poly(sodium-pstyrenesulfonate); PILs, polymeric ionic liquids; GP, graphene; $CoFe_2O_4$, cobalt ferrite; MoS_2, molybdenum disulfide; Au NPs, gold nanoparticles; TiO_2, titanium dioxide.

3.4. Selectivity, Stability, and Reproducibility Assays

Selectivity is essential for reliable analyte determination, particularly in complex samples with numerous potentially interfering species, such as glucose, AA, fructose, DA, sucrose, UA, and L-Cyst. These potential interfering species were selected to provide an initial evaluation of the biosensor response in the presence of common biomolecules and electroactive compounds. These species represent compounds that may be encountered in biological samples or could influence electrochemical measurements. The selectivity of the Nf/ChOx/ZnO NSs/Ag/Si biosensor was evaluated using DPV measurements over a potential range of +0.1–+0.7 V by separately introducing 100 µM of each analyte (glucose, AA, fructose, DA, sucrose, UA, L-Cyst, cholesterol) along with all the above interfering species (100 µM) in the buffer (Figure 7a). The DPV response showed no peaks in the buffer and in the presence of potential interfering substances. However, the biosensor showed a pronounced DPV current response to cholesterol, whereas adding all interferents together produced negligible changes in the recorded signal (Figure 7b). This excellent selectivity is primarily attributed to the high substrate specificity of ChOx, which preferentially catalyzes cholesterol oxidation while showing no interaction with the tested interferents. Furthermore, the Nf membrane can contribute to selective detection by facilitating cholesterol transport while restricting the diffusion of certain potentially interfering species based on their molecular size and charge [52]. The combination of enzyme-specific recognition and the selective Nf barrier therefore minimizes nonspecific electrochemical responses, resulting in reliable and accurate cholesterol determination. These findings demonstrate the robustness of the Nf/ChOx/ZnO NSs/Ag/Si biosensor and support its potential application for cholesterol analysis in complex samples.

The fabrication reproducibility of the Nf/ChOx/ZnO NSs/Ag/Si biosensor was investigated using five independently fabricated electrodes for the DPV determination of 100 µM cholesterol, as shown in Figure 7c. The cholesterol biosensor electrodes showed highly comparable current responses, yielding an RSD of ~2.4% and confirming good electrode-to-electrode reproducibility. We further examined the biosensor's operational stability by recording its response over a 10-week storage period (Figure 7d). After 10 weeks, the biosensor retained approximately 92% of its initial response, demonstrating excellent long-term stability. The excellent stability can be associated with the direct growth of vertically aligned, elongated cone-shaped ZnO NSs on the seeded Ag/Si electrode, which provides strong interfacial attachment and a large accessible surface for efficient enzyme

immobilization [53]. The robust nanostructured architecture helps minimize enzyme loss and maintains effective electron-transfer pathways, thereby contributing to the prolonged sensing performance of the fabricated biosensor.

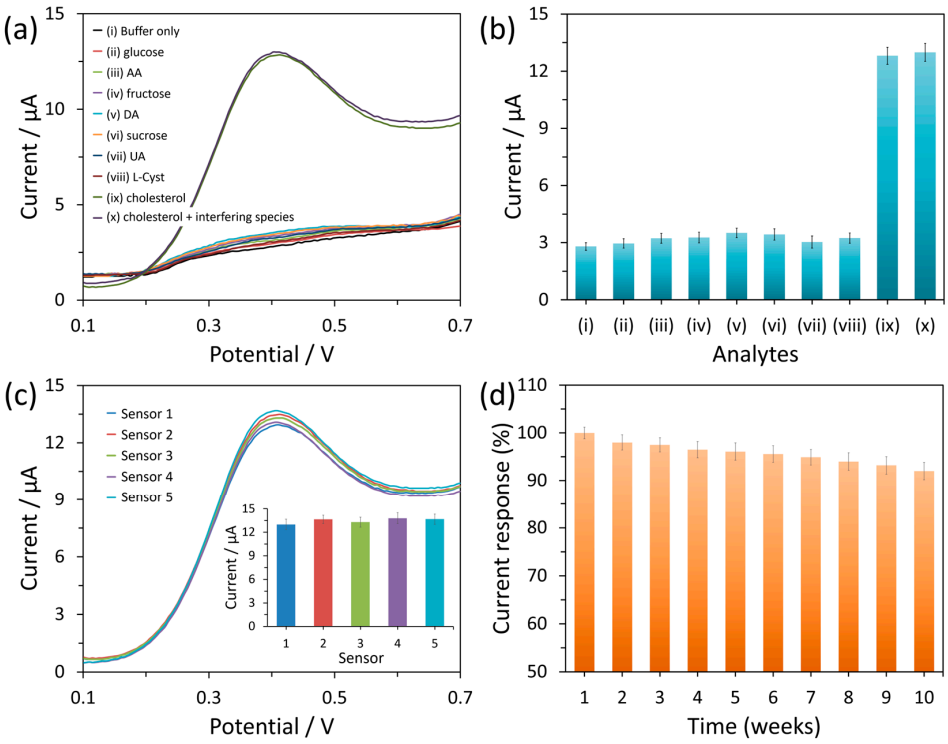

Figure 7. (**a**) Selectivity analysis of the Nf/ChOx/ZnO NSs/Ag/Si biosensor in the buffer (i) with 100 µM of each analyte, i.e., glucose (ii), AA (iii), fructose (iv), DA (v), sucrose (vi), UA (vii), L-Cyst (viii), cholesterol (ix), and 100 µM cholesterol along with all the above interfering species (100 µM) (x). (**b**) Histogram showing DPV response for each analyte. (**c**) Reproducibility test of the five identical biosensors (Nf/ChOx/ZnO NSs/Ag/Si) fabricated using the same fabrication procedure and measuring their DPV response for 100 µM cholesterol (inset shows the response histogram with RSD of ~2.4%). (**d**) Stability test of the Nf/ChOx/ZnO NSs/Ag/Si biosensor for 10 weeks.

3.5. Applicability of Biosensor in Serum Sample

The applicability of the fabricated Nf/ChOx/ZnO NSs/Ag/Si biosensor was evaluated by determining cholesterol levels in human serum (H4522; Sigma-Aldrich, Burlington, MA, USA). We diluted the commercial human serum (Sigma-Aldrich, H4522; cholesterol concentration 5.2 mM) 20-fold before electrochemical analysis [54,55]. The diluted serum ensured the cholesterol concentration fell within the sensor's validated linear detection range of 5–600 µM. Cholesterol standards (50–200 µM) were then added to the diluted serum using the standard addition method. The selected spike concentrations were chosen to maintain the final cholesterol concentrations within the linear calibration range. The cholesterol concentration in each sample was determined from the corresponding calibration response, accounting for the dilution factor and added cholesterol. The percentage recovery was calculated using [Recovery (%) = (measured concentration in the spiked sample—concentration in unspiked diluted serum/spiked cholesterol concentration) × 100]. The RSD values were calculated from three replicate measurements. The recovery values ranged from 94.5–96.6%, with an RSD of 4.6–5.5%, indicating satisfactory agreement and repeatability (Table 2). These results demonstrate the Nf/ChOx/ZnO NSs/Ag/Si biosensor's satisfactory analytical performance in buffer and preliminary spike-recovery experiments using human serum. However, these results represent an initial assessment of its potential for real-sample analysis. The present study does not include comprehensive validation using clinical

samples or comparison with established laboratory methods. Future studies involving a larger sample cohort, assessment of sample-to-sample variability, and comparison with standard cholesterol assays will be necessary to establish the biosensor's analytical reliability and practical applicability.

Table 2. Cholesterol detection in diluted serum sample using our fabricated biosensor.

Sample	Spiked (μM)	Detected (μM)	Recovery (%)	RSD (%) (n = 3)
Human serum (20-fold diluted in PBS)	0	256	-	-
	50	303.25	94.5	4.6
	100	351.2	95.2	4.9
	200	449.2	96.6	5.5

4. Conclusions

In this study, we synthesised elongated, cone-shaped ZnO NSs via a hydrothermal approach and grew them directly on an Ag electrode, yielding a uniform, tilted architecture. The distinctive elongated, tilted, cone-like morphology provided a favorable platform for enzyme immobilization and facilitated efficient electron transfer, contributing to the enhanced analytical performance of the resulting Nf/ChOx/ZnO NSs/Ag/Si cholesterol biosensor. The developed device exhibited a broad linear detection range extending up to 600 μM and a high sensitivity of 0.398 μA μM^{-1} cm^{-2}, demonstrating its capability for sensitive cholesterol determination. The proposed ZnO-based electrochemical sensor demonstrated promising cholesterol-detection performance, including satisfactory interference resistance, storage stability, and preliminary spike-recovery results in human serum. These findings support its potential for further development in cholesterol sensing. Nevertheless, establishing clinical applicability requires comprehensive validation using a larger set of real serum samples and direct comparison with established analytical methods. Overall, the elongated cone-shaped ZnO nanostructures provide a promising nanostructured approach for enzymatic cholesterol sensing. Further integration with modified nanomaterials and flexible conductive substrates may expand this platform's potential applications in wearable and point-of-care sensing technologies. However, such applications will require additional analytical and practical validation.

Author Contributions: Conceptualization, K.H. and R.A.; methodology, R.A. and A.; software, K.H., R.A. and V.N.; validation, V.N., A. and K.S.B.; formal analysis, K.H., K.S.B., A. and A.A.; investigation, R.A., V.N., K.S.B., A., A.A. and M.B.A.; resources, B.-I.L.; data curation, R.A., V.N., A.A. and K.S.B.; writing—original draft preparation, K.H. and R.A.; writing—review and editing, R.A., K.S.B., A.A., M.B.A. and B.-I.L.; visualization, R.A.; supervision, B.-I.L.; project administration, B.-I.L.; funding acquisition, B.-I.L. All authors have read and agreed to the published version of the manuscript.

Funding: This work was supported by the Global Joint Research Program funded by the Pukyong National University (202607540001). A.A. and M.B.A. acknowledge the generous support from Prince Sattam Bin Abdulaziz University project number (PSAU/2025/R/1447).

Data Availability Statement: Data presented in this study are available from the corresponding author.

Conflicts of Interest: The authors declare no conflicts of interest.

References

1. Subczynski, W.K.; Pasenkiewicz-Gierula, M.; Widomska, J.; Mainali, L.; Raguz, M. High cholesterol/low cholesterol: Effects in biological membranes: A Review. *Cell Biochem. Biophys.* **2017**, *75*, 369–385. [CrossRef]
2. Cui, D.; Yu, X.; Guan, Q.; Shen, Y.; Liao, J.; Liu, Y.; Su, Z. Cholesterol metabolism: Molecular mechanisms, biological functions, diseases, and therapeutic targets. *Mol. Biomed.* **2025**, *6*, 72. [CrossRef]
3. Hansen, S.B.; Wang, H. The shared role of cholesterol in neuronal and peripheral inflammation. *Pharmacol. Ther.* **2023**, *249*, 108486. [CrossRef]
4. Mihaylova, B.; Emberson, J.; Blackwell, L.; Keech, A.; Simes, J.; Barnes, E.H.; Voysey, M.; Gray, A.; Collins, R.; Baigent, C. The effects of lowering LDL cholesterol with statin therapy in people at low risk of vascular disease: Meta-analysis of individual data from 27 randomised trials. *Lancet* **2012**, *380*, 581–590. [CrossRef]
5. Abdelhamid, A.S.; Brown, T.J.; Brainard, J.S.; Biswas, P.; Thorpe, G.C.; Moore, H.J.; Deane, K.H.; AlAbdulghafoor, F.K.; Summerbell, C.D.; Worthington, H.V.; et al. Omega-3 fatty acids for the primary and secondary prevention of cardiovascular disease. *Cochrane Database Syst. Rev.* **2020**, *3*, CD003177. [CrossRef]
6. Simon, K.C.; Chen, H.; Michael, S.; Ascherio, A. Hypertension, hypercholesterolemia, diabetes, and risk of Parkinson disease. *Neurology* **2007**, *69*, 1688. [CrossRef]
7. Elmehdawi, R. Hypolipidemia: A word of caution. *Libyan J. Med.* **2008**, *3*, 84. [CrossRef]
8. Gill, P.K.; Hegele, R.A. Low cholesterol states: Clinical implications and management. *Expert Rev. Endocrinol. Metab.* **2023**, *18*, 241–253. [CrossRef]
9. Xu, S.; Wang, Y.; Zhou, D.; Kuang, M.; Fang, D.; Yang, W.; Wei, S.; Ma, L. A novel chemiluminescence sensor for sensitive detection of cholesterol based on the peroxidase-like activity of copper nanoclusters. *Sci. Rep.* **2016**, *6*, 39157. [CrossRef]
10. Li, L.H.; Dutkiewicz, E.P.; Huang, Y.C.; Zhou, H.B.; Hsu, C.C. Analytical methods for cholesterol quantification. *J. Food Drug Anal.* **2018**, *27*, 375–386. [CrossRef]
11. Abed, H.; Sabouni, R.; Ghommem, M.; Azam, M.U.; Askar, K.; Alcheikh, N. FeBTC as peroxidase mimic for colorimetric cholesterol detection. *Sci. Rep.* **2025**, *16*, 2777. [CrossRef]
12. Zhou, Z.; Zong, J.; Xu, N. Review of methods for the determination of cellular cholesterol content: Principles, advantages, limitations, applications, and perspectives. *Anal. Sci.* **2025**, *41*, 1697–1714. [CrossRef]
13. Ndhlala, A.R.; Yüksel, A.K.; Çelebi, N.; Doğan, H.O. A general review of methodologies used in the determination of cholesterol ($C_{27}H_{46}O$) levels in foods. *Foods* **2023**, *12*, 4424. [CrossRef]
14. Cunha, D.R.; Quinaz, M.B.; Segundo, M.A. Biopharmaceutical analysis—Current analytical challenges, limitations, and perspectives. *Anal. Bioanal. Chem.* **2025**, *418*, 373. [CrossRef]
15. Aslam, M.; Bhola, R.; Anadebe, V.C.; Shukla, S.; Ebenso, E.E.; Kumari, K.; Meghvansi, M.K.; Singh, P. Advanced nanomaterials for dehydrogenase-based electrochemical sensing: A comprehensive review. *Sens. Actuators Rep.* **2026**, *12*, 100494. [CrossRef]
16. Jasper, I.; da Rocha Rodrigues, R.; Florencio, J.C.; Sauer, H.; Hryniewicz, B.M.; Vidotti, M. Recent advances and emerging strategies of electrochemical sensors for pesticides and toxic metals detection. *Discov. Sens.* **2026**, *2*, 23. [CrossRef]
17. Zhu, C.; Yang, G.; Li, H.; Du, D.; Lin, Y. Electrochemical sensors and biosensors based on nanomaterials and nanostructures. *Anal. Chem.* **2015**, *87*, 230–249. [CrossRef]
18. Chowdhury, A.D.; Sarkar, S.; Dasgupta, U.; Ghosh, M. Nanostructured electrochemical biosensors for real-time and portable health monitoring systems. *Biosens. Bioelectron. X* **2026**, *30*, 100766. [CrossRef]
19. Ahmad, R.; Lee, B. Facile fabrication of palm trunk–like ZnO hierarchical nanostructure–based biosensor for wide-range glucose detection. *Chem. Eng. J.* **2024**, *492*, 152432. [CrossRef]
20. Kalambate, P.K.; Pansare, A.V.; Ashamary, F.; Sivasurya, E.; Pokhrel, S.; Boddula, R.; Manoj, D. Attomolar and beyond: Ultrasensitive electrochemical biosensors for next-generation detection. *TrAC Trends Anal. Chem.* **2026**, *197*, 118726. [CrossRef]
21. Ahmad, R.; Mahmoudi, T.; Ahn, M.S.; Hahn, Y.B. Recent advances in nanowires-based field-effect transistors for biological sensor applications. *Biosens. Bioelectron.* **2018**, *100*, 312–325. [CrossRef]
22. Ahmad, R.; Wolfbeis, O.S.; Hahn, Y.B.; Alshareef, H.N.; Torsi, L.; Salama, K.N. Deposition of nanomaterials: A crucial step in biosensor fabrication. *Mater. Today Commun.* **2018**, *17*, 289–321. [CrossRef]
23. Shan, X.; Jia, X.; Chen, J.; Gao, S.; Zhang, Y.; Hu, G. Emerging inorganic nanomaterial-based electrochemical sensors for heavy metal detection in food: Advances, challenges, and prospects. *Curr. Res. Food Sci.* **2025**, *12*, 101346. [CrossRef]
24. Petković, B.B.; Ognjanović, M.; Stanković, D.M. Recent progress in nanomaterials for electrochemical sensing of natural bioactive compounds. *Chemosensors* **2025**, *13*, 429. [CrossRef]
25. Hahn, Y.B.; Ahmad, R.; Tripathy, N. Chemical and biological sensors based on metal oxide nanostructures. *Chem. Commun.* **2012**, *48*, 10369–10385. [CrossRef]
26. Ahmad, M.; Nisar, A.; Sun, H. Emerging trends in non-enzymatic cholesterol biosensors: Challenges and advancements. *Biosensor* **2022**, *12*, 955. [CrossRef]

27. Ahmed, M.M.; Xu, Q. Recent advances in ZnO-based electrochemical sensors for food safety monitoring. *Anal. Biochem.* **2026**, *712*, 116049. [CrossRef]
28. Zhang, X.; Cai, X.; Yin, N.; Che, Y.; Jiao, Y.; Zhang, C.; Yu, J.; Liu, C. Hierarchical PVDF/ZnO/Ag/ZIF-8 nanofiber membrane used in trace-level Raman detection of H_2S. *J. Hazard. Mater.* **2024**, *471*, 134441. [CrossRef]
29. Krishna, M.S.; Singh, S.; Batool, M.; Fahmy, H.M.; Seku, K.; Shalan, A.E.; Lanceros-Mendez, S.; Zafar, M.N. A review on 2D-ZnO nanostructure based biosensors: From materials to devices. *Mater. Adv.* **2023**, *4*, 320–354. [CrossRef]
30. Dassallem, S.; Nouneh, K.; Xue, Y.; Tonelli, D.; Taleb, A. A review on hierarchical nanostructures for electrochemical sensors. *Sensors* **2025**, *26*, 73. [CrossRef]
31. Yan, L.; Zhang, X.; Lv, D.; Liu, Z.; Yang, F.; Gao, Y.; Wang, X.; Jiang, Y.; Zhao, B. Sensing of the charge transfer process in ZnO/$MAPbI_3$ heterojunctions of perovskite solar cells (PSCs) by surface-enhanced Raman scattering. *J. Mater. Chem. C* **2023**, *11*, 9179–9188. [CrossRef]
32. Liu, G.; Wang, L.; Gao, Z.; Feng, C.; Liu, Q.; Chen, X. Interfacially crystallized Enzyme@MOFs biocatalytic membranes for highly efficient synthesis of D-amino acids via continuously recirculating stereoinversion. *Chem. Eng. J.* **2024**, *497*, 154529. [CrossRef]
33. Liu, G.; Wang, L.; Zhu, F.; Liu, Q.; Feng, Y.; Zhao, X.; Chen, M.; Chen, X. Facile construction of a reusable multi-enzyme cascade bioreactor for effective fluorescence discrimination and quantitation of amino acid enantiomers. *Chem. Eng. J.* **2022**, *428*, 131975. [CrossRef]
34. Man, B.; Wang, G.; Li, Z.; Xu, S.; Li, C.; Yu, J.; Zhang, C.; Zhao, X. MoS_2-spaced bimetal composite structure as SERS-SPR sensor for glucose detection. *J. Alloys Compd.* **2022**, *902*, 163789. [CrossRef]
35. Ahmad, R.; Bhat, K.S.; Nagal, V.; Nakate, U.T.; Ahmad, A.; Alshammari, M.B.; Alam, S.; Lee, B.I. Surface-engineered vertically-aligned ZnO nanorod for sensitive non-enzymatic electrochemical monitoring of cholesterol. *Heliyon* **2024**, *10*, e37847. [CrossRef]
36. Sushmitha, S.; Hegde, S.S.; Rao, L.; Varsha, G.; Bhat, B.R. Advancements in nonenzymatic electrochemical cholesterol detection: Fostering material innovation with biosensing technologies. *Sens. Diagn.* **2026**, *5*, 8–25. [CrossRef]
37. Xiang, R.; Wang, C.; Luo, W.; Gao, Q. Perspective on recent advances in self-supported electrodes with hierarchical structures for efficient and durable water electrolysis. *Dalton Trans.* **2025**, *54*, 17730–17753. [CrossRef]
38. Bakry, M.; Ismail, W.; Abdelfatah, M.; El-Shaer, A. Low-cost fabrication methods of ZnO nanorods and their physical and photoelectrochemical properties for optoelectronic applications. *Sci. Rep.* **2024**, *14*, 23788. [CrossRef]
39. Ahmad, R.; Tripathy, N.; Jang, N.K.; Khang, G.; Hahn, Y.B. Fabrication of highly sensitive uric acid biosensor based on directly grown ZnO nanosheets on electrode surface. *Sens. Actuators B Chem.* **2014**, *206*, 146–151. [CrossRef]
40. Bhat, K.S.; Ahmad, R.; Mahmoudi, T.; Hahn, Y.B. High performance chemical sensor with field-effect transistors array for selective detection of multiple ions. *Chem. Eng. J.* **2021**, *417*, 128064. [CrossRef]
41. Sidhu, M.S.; Sridharan, G.; Ganapathy, D.; Atchudan, R.; Arya, S.; Mahadevegowda, S.H.; Sundramoorthy, A.K. Development of highly sensitive electrochemical biosensor for the detection of hydroquinone using a FAD functionalized fluorapatite/SWCNT hybrid composite modified electrode. *RSC Adv.* **2025**, *15*, 17829–17842. [CrossRef]
42. Shah, A.; Ahmad, M.; Rahmanuddin; Khan, S.; Aziz, U.; Ali, Z.; Khan, A.; Mahmood, A. The role of Al doping on ZnO nanowire evolution and optical band gap tuning. *Appl. Phys. A* **2019**, *125*, 713. [CrossRef]
43. Sanginario, A.; Hernández, S. Diagnostics of electrocatalytic systems by electrochemical impedance spectroscopy. *Curr. Opin. Green Sustain. Chem.* **2023**, *39*, 100727. [CrossRef]
44. Demkiv, O.; Nogala, W.; Stasyuk, N.; Grynchyshyn, N.; Vus, B.; Gonchar, M. The peroxidase-like nanocomposites as hydrogen peroxide-sensitive elements in cholesterol oxidase-based biosensors for cholesterol assay. *J. Funct. Biomater.* **2023**, *14*, 315. [CrossRef]
45. Batra, N.; Tomar, M.; Gupta, V. ZnO-CuO composite matrix based reagentless biosensor for detection of total cholesterol. *Biosens. Bioelectron.* **2015**, *67*, 263–271. [CrossRef]
46. Xia, T.; Liu, G.; Wang, J.; Hou, S.; Hou, S. MXene-based enzymatic sensor for highly sensitive and selective detection of cholesterol. *Biosens. Bioelectron.* **2021**, *183*, 113243. [CrossRef]
47. Rahman, M.M.; Li, X.; Kim, J.; Lim, B.O.; Ahammad, A.S.; Lee, J. A cholesterol biosensor based on a bi-enzyme immobilized on conducting poly(thionine) film. *Sens. Actuators B Chem.* **2014**, *202*, 536–542. [CrossRef]
48. Zhu, L.; Xu, L.; Tan, L.; Tan, H.; Yang, S.; Yao, S. Direct electrochemistry of cholesterol oxidase immobilized on gold nanoparticles-decorated multiwalled carbon nanotubes and cholesterol sensing. *Talanta* **2013**, *106*, 192–199. [CrossRef]
49. Wu, S.; Wang, Y.; Mao, H.; Wang, C.; Xia, L.; Zhang, Y.; Ge, H.; Song, X.M. Direct electrochemistry of cholesterol oxidase and biosensing of cholesterol based on PSS/polymeric ionic liquid–graphene nanocomposite. *RSC Adv.* **2016**, *6*, 59487–59496. [CrossRef]
50. Ayyandurai, N.; Venkatesan, S.; Raman, S. A sensitive enzymatic electrochemical biosensor for cholesterol based on cobalt ferrite@molybdenum disulfide/gold nanoparticles. *ACS Appl. Bio Mater.* **2024**, *7*, 4080–4092. [CrossRef]
51. Kariz, D.G.A.; Darabi, E.; Elahi, S.M. Electrochemical sensing of cholesterol based on MWCNTs loaded nanoparticles. *Int. Nano Lett.* **2022**, *12*, 113–123. [CrossRef]

52. Kariz, D.G.A.; Darabi, E.; Elahi, S.M. Fabrication of Au/ZnO/MWCNTs electrode and its characterization for electrochemical cholesterol biosensor. *J. Theor. Appl. Phys.* **2020**, *14*, 339–348. [CrossRef]
53. Zhai, C.; Zhang, K.; Liu, Y.; Xia, S. Enhancing selectivity of nanofiltration membranes for mineral ions and per- and polyfluoroalkyl substances via dual-component-assisted interfacial polymerization. *Water Res.* **2025**, *287*, 124315. [CrossRef]
54. Ahmad, R.; Majhi, S.M.; Zhang, X.; Swager, T.M.; Salama, K.N. Recent progress and perspectives of gas sensors based on vertically oriented ZnO nanomaterials. *Adv. Colloid Interface Sci.* **2019**, *270*, 31154073. [CrossRef]
55. Kodaira, K.; Kuramitz, H.; Sugawara, K. Designing a peptide-modified screen-printed gold electrode as a sensor for the human monocytic leukemia cell line. *Electroanalysis* **2023**, *35*, e202200204. [CrossRef]

Disclaimer/Publisher's Note: The statements, opinions and data contained in all publications are solely those of the individual author(s) and contributor(s) and not of MDPI and/or the editor(s). MDPI and/or the editor(s) disclaim responsibility for any injury to people or property resulting from any ideas, methods, instructions or products referred to in the content.